A DEM APPROACH FOR MODELING BIOMASS FAST PYROLYSIS IN A DOUBLE AUGER REACTOR

Fenglei Qi[1]

[1] Faculty of Science, Technology and Communication, University of Luxembourg
Maison du Nombre, 6 Avenue de la Fonte, 4364 Esch-sur-Alzette, Luxembourg
fenglei.qi@uni.lu

Keywords DEM, biomass pyrolysis, auger reactor, biomass granules

Abstract Thermochemical conversion of biomass via fast pyrolysis process is a promising way to produce renewable fuels and chemicals. In this paper, an extended discrete element method (DEM) is developed to predict the biomass fast pyrolysis process in a double auger reactor, which is described as a reacting granular flow. The thermodynamic state of each particle is properly predicted with an addition of a heat transfer model and a reaction model on top of the traditional DEM method. The results suggest that the predictions of the thermochemical decomposition kinetics of biomass components are consistent with the experimental observations. The results also indicate that the fast pyrolysis in the reactor is controlled by the heat transfer process. Any operating condition variation in favor of enhancing heat transfer is beneficial to the fast pyrolysis process and vice versa.

1 INTRODUCTION

Biomass is a low-carbon renewable resource that has been used for thousands of years to provide heat and energy in rural areas. More efficient and clean ways of utilizing biomass such as fast pyrolysis are being promoted in recent decades [1, 2, 3]. Biomass fast pyrolysis is achieved at reaction temperature of around 500 °C and atmospheric pressure in the absence of oxygen. Three products including bio-oil (tar), char and non-condensable gas are generated in the process and their mass-based percentage are around 65%, 15% and 20%, respectively. Chemicals and fuels are targeted products through upgrade processing of bio-oil. The yield of bio-oil, char and non-condensable gas is usually subject to changes of feedstock type, reactor temperature as well as heat and mass transport process in the reactor. Understanding the various parameter influences on the biomass pyrolysis process is an essential step for the reactor design and process optimization.

Auger reactors are one of the commonly used reactors for biomass fast pyrolysis [4, 5]. In an auger reactor, the mechanical force is provided to the bed to enhance particle mixing and heat transfer, and facilitate particulate matter transport for continuous operation. The pyrolysis process in the auger reactor configuration is a reactive granular flow system

which involves particle flow, heat transfer and biomass devolatilization reactions at the same time. Although several modeling approaches [6, 7, 8, 9] have been employed to predict particle mixing, heat transfer and pyrolysis, the reactor-scale evaluation of the heat and mass transfer effects on the biomass fast pyrolysis is still very limited.

In this contribution, we propose an extended discrete element method (DEM) for modeling reactive granular flows in the double auger reactor. The developed approach simulates the evolution of the particle thermodynamic state in terms of temperature and compositions, which are predicted with a heat transfer model and a reaction model. The following section describes the double auger reactor system and presents the simulation approach. Thereafter, the results are presented, showing the capability of the developed approach and the comparison of prediction results and experimental observations.

2 MODEL DESCRIPTION

2.1 Double auger reactor

The geometry of the double auger reactor is shown in Figure 1, which has the same dimension as used in the experimental study by Brown and Brown [10]. Two augers are installed in the trough. The left auger flight is left-handed and the right auger flight is right-handed. As show in Figure 1 (a), when the left auger is rotating in the clockwise direction and the right screw is rotating in the counter-clockwise direction, the bulk material is pushed forwards from the inlet side to the outlet side along the axial direction. There are two inlets which separately feed biomass particles (red oak) at the inlet 1 and heat carrier particles (sand) at inlet 2 as shown in Figure 1 (a). The biomass particle has a particle size range of 300-710 μm in the experiments and is fed into the system at the ambient temperature. The sand particle either has a particle range of 250-600 μm (fine sand) or 600-1000 μm (coarse sand) in the experiments and is fed into the system at high temperature depending on the reaction temperature requirement. The screw rotation speed varied from 20 RPM to 60 RPM in the operation of the reactor [10].

2.2 DEM approach

The approach is composed of three parts: a spring-dashpot model accounting for particle contact dynamics, a heat transfer model for conductive and radiative heat transfer among particles as well as potential convective heat transfer with an interacting fluid, and a reaction model for the biomass devolatilization. The contact dynamic model and the heat transfer model have been presented in our previous studies [6, 7]. In this paper, the description of the approach only focuses on the reaction model and the time step coordination algorithm between the reaction model and DEM.

2.3 Mass balance equation

Biomass is originally composed of four major components: hemicellulose, cellulose, lignin and liquid species. Liquid species mainly include the different forms of water [11]

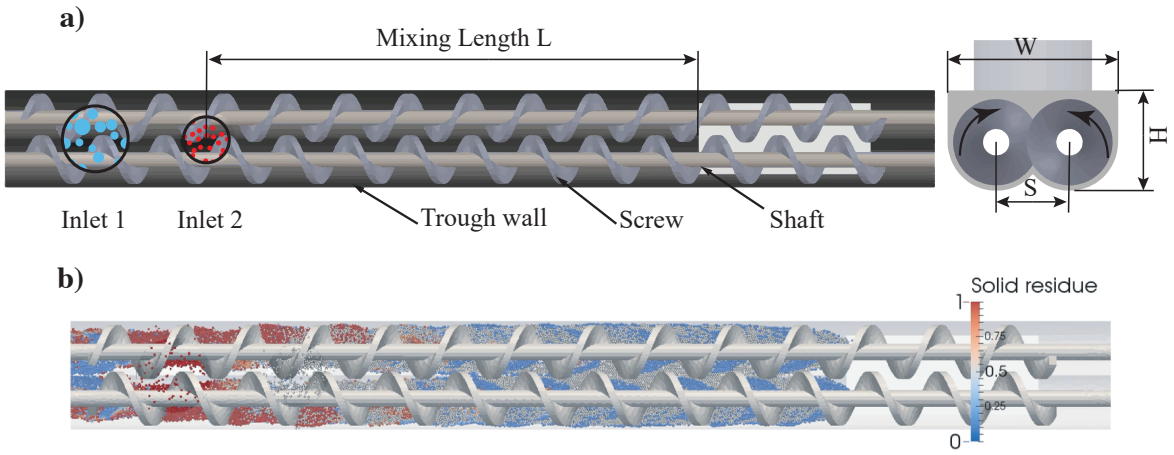

Figure 1: (a) Geometry of the double auger reactor and (b) Biomass solid residue prediction. Biomass particles are fed into the reactor at inlet 1 and sand particles are fed into the reactor at inlet 2. The ratio of the length L to the screw flight diameter D is 10. The ratio of the screw pitch P to the screw flight diameter D is 1.25. Both biomass and sand sizes in (b) are 2 mm and the augers rotate at the speed of 40 RPM.

in the biomass matrix. In the pyrolysis process, solid, liquid and gas species are involved and a variety of intermediate species are produced and consumed. The particle mass is composed of all solid species and liquids including biomass original components, intermediate solid species, solid products and liquid water. Gaseous species include products such as water vapor, non-condensable gases and tar vapor. The produced water vapor, non-condensable gas and tar vapor emit for the particle surface immediately and cause the reduction of particle mass. In the pyrolysis of a biomass particle, the conversion process progresses gradually into the biomass core from outside. However, in the current approach, the mass loss of the biomass particle is considered uniform across the particle. In addition, we focus on the thermochemical decomposition dynamics of the solid components in the reactor, the secondary reactions in the gaseous phase and the heterogeneous reactions between gas phase and solid phase are not involved in current model. The mass change rate of particle i is formulated as

$$\frac{dm_i}{dt} = \frac{dm^p_{water}}{dt} - \dot{r}_{gas} - \dot{r}_{tar}, \tag{1}$$

where, the first term on the right hand side accounts for the water evapation from the particle, and $\dot{r}_{gas}$, $\dot{r}_{tar}$ are the production rates for non-condensable gas and tar arising from the biomass pyrolysis.

For solid species, the mass balance is written as

$$\frac{\partial m^p_{si}}{\partial t} = \dot{r}_{si} \quad i = 1, \ldots, n_s, \tag{2}$$

where, m_{si}^p is the mass of solid species i in the particle, $\dot{r}_{si}$ is the net production rate of the solid species. For liquid phase, a similar mass balance is written as

$$\frac{\partial m_{li}^p}{\partial t} = \dot{r}_{li} \quad i = 1, \ldots, n_l, \tag{3}$$

where, m_{li}^p is the mass of liquid species i in the particle, $\dot{r}_{li}$ is the net production rate of liquid species i . For vapor species, the accumulating mass is calculated from

$$\frac{\partial m_{vi}}{\partial t} = \dot{r}_{vi} \quad i = 1, \ldots, n_v, \tag{4}$$

and m_{vi} is the accumulated mass of gaseous species i emitted from a particle, $\dot{r}_{vi}$ is the net production rate of gaseous species.

2.4 Pyrolysis kinetics

Adopting mechanistic kinetics could provide detailed reaction information of the biomass devolatilization process but requires extensive computational time. In the consideration of both reaction details and computational time, a multiple-component reaction scheme proposed by Calonaci et al. [12] is adopted. The biomass pyrolysis is modeled via a superposition of hemicellulose, cellulose and lignin. The reaction pathway is illustrated in Figure 2 and the reaction parameters can be founded in [12]. In this paper, we focus on the biomass primary devolatilization, the secondary reactions occurring in the gas phase are not modeled.

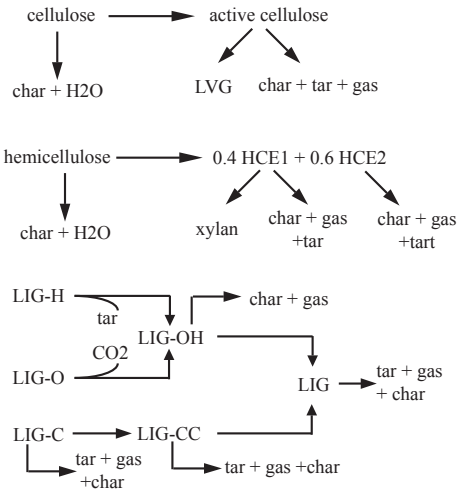

Figure 2: Illustration of the biomass pyrolysis scheme developed in [12].

All the reactions in the biomass pyrolysis scheme are of first order. The reaction rate of reaction r is written as

$$\dot{w}_r = A_r \exp\left(-\frac{E_r}{RT_p}\right) m_r^p, \tag{5}$$

where, A_r, E_r and R are the frequency factor, activate energy and gas constant for reaction r, $m_{p,r}$ is the mass of reactant in the particle. The production rate of each species is thereafter written in terms of reaction rate $\dot{w}_r$ accordingly.

2.5 Particle properties

In the biomass pyrolysis process, biomass properties such as particle porosity and thermal conductivity are functions of biomass conversion process and temperature. Biomass conversion is formulated as

$$X = 1 - \frac{m_b}{m_{b,0}}, \tag{6}$$

where, $m_{b,0}$ is the initial biomass mass. The biomass particle thermal conductivity is written as

$$k_{p,b} = (1 - X)\, k_b + X k_{char}. \tag{7}$$

In the equation, k_b and k_{char} refer to the biomass and char (solid product) conductivities, respectively. The conductivities of biomass and char remained 0.2 and 0.1 W/(mK). The specific heat capacities for biomass and char are [13]:

$$c_{p,b} = 1500 + T_p, \tag{8}$$

$$c_{p,char} = 420 + 2.09T_p + 6.85 \times 10^{-4} T_b^2. \tag{9}$$

The other parameter values employed in the simulations are listed in Table 1.

2.6 Numerical algorithms

The implementation of the extended DEM is based on LIGGGHTS software [14]. A fixed time step of 2.5×10^{-6} s for updating particle position and temperature is adopted which could guarantee the time step is less than 20% of the critical time step determined from the Rayleigh wave speed of force transmission in the bed. The critical time is formulated as

$$\Delta t = \frac{\pi R}{0.8766 + 0.1631\nu} \sqrt{\frac{\rho}{G}}. \tag{10}$$

The Verlet integration method is adopted for integrating particle motion equations. The runge-kutta-dopri5 ODE solver from the odeint code [15] is incorporated in the algorithm to integrate the reaction ODEs. The time step for the ODE integration is adaptive as shown in Figure 3. Reaction integration time step is reduced when the temperature change due to the heat of reaction source in one integration time step exceeds a set point. Significant amount of heat sink or source was found to cause a stability issue in

Table 1: Biomass and sand properties in DEM

Material*	Red oak (dry)	Sand	Steel
Material mechanical properties			
Initial Density ρ (kg/m^3)	500	2680	-
Diameter d_p (mm)	2 mm	2 mm	-
Young's Modulus E (Pa)	6.0×10^6	6.0×10^6	6.0×10^6
Original Young's Modulus E_o (Pa)	1.2×10^{10}	7.0×10^{10}	2.0×10^{11}
Poisson's ratio ν	0.29	0.25	0.3
Coefficient of restitution e †	0.4	0.65	0.65
Coefficient of friction μ		0.2	
Coefficient of rolling friction μ_r		1×10^{-4}	
Material thermal properties			
Initial Temperature T_0 (K)	300	848	788
Conductivity k $\left(\frac{\text{W}}{\text{m}\cdot\text{K}}\right)$ ‡	0.2	1.3	38
Specific heat capacity c_p $\left(\frac{\text{W}}{\text{kg}\cdot\text{K}}\right)$	$1500 + T_p$	730	490
Emissivity ϵ_r	0.9	0.8	0.8

* Red oak is the material for biomass particles and sand for heat carrier particles. Steel is used for reactor structures.
† This row shows the coefficient of restitution between the same material. The coefficient between red oak and sand is 0.4. The coefficient between red oak and steel is 0.4. The coefficient between sand and steel is 0.65.
‡ The fluid thermal conductivity is 0.039 W/m · K.

the temperature prediction from the energy equation. The proposed adaptive time step method could prevent the stability issue and reduce the computational burden of adopting a smaller fixed time step for all the particles in the whole simulation time.

3 RESULTS AND DISCUSSION

As mentioned in the Introduction section, the biomass fast pyrolysis process is influenced by the operating conditions of the reactor (screw rotation speed, heat carrier sand

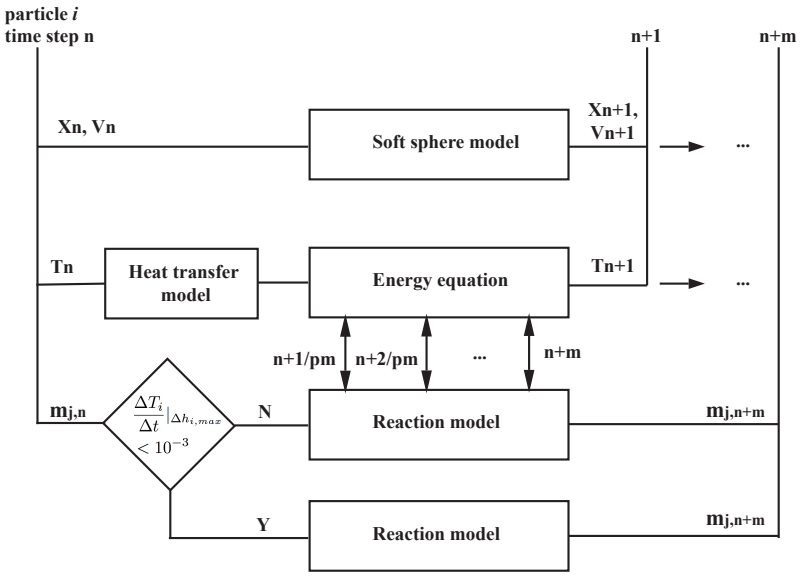

Figure 3: Implemented algorithm of adaptive time step size for the reaction model. The reaction model takes $m\Delta t$ time step size at the beginning of each integration, where Δt is the DEM time step size. If the integration condition $\Delta T_i/\Delta t_r|_{\Delta h_i} < 10^{-3}$ is not met, the integration time step size Δt_r for the reaction model is decreased by half and the time step reduction continues recursively until the integration condition is met. p is the resultant number of steps for reaction integration within $m\Delta t$ time.

temperature and fill level) and the biomass properties such as feestock type, particle size and moisture content. The prediction accuracy also subjects to the adopted pyrolysis reaction kinetics. In this short paper, it's not intended to present detailed parameter study but to show the capability of the developed approach in modeling biomass fast pyrolysis process. Herein, the screw rotation speed is fixed at 40 RPM and the sand inlet temperature is 848 K. The size of both biomass and sand particles is 2 mm diameter. Moisture content is set to 10 wt% dry biomass. Following the same approach, the parameter study can be easily carried out.

3.1 Biomass particle temperature and mass loss

The heat of pyrolysis is found to have a significant impact on the biomass pyrolysis process in the reactor. To show the influence, two simulations were carried with and without the heat of pyrolysis, and the profiles of temperature and mass loss are plotted in Figure 4. As expected, the biomass temperature is gradually heated up as the biomass is transported in the axial direction by the augers in both cases. However, the degree of the pyrolysis process is noticeably different. With a careful examination, it is observed that both temperature and mass residue profiles are similar with and without the heat source from fast pyrolysis reactions before $x/D = 6$. After $x/D = 6$, the biomass temperature

profile slope decreases when the heat of pyrolysis is included. The reduction of the temperature slope is consistent with the experimental observation in [16], stating that the endothermic decomposition reactions of cellulose start at 588 K. The biomass temperature profile slope decreases after $x/D = 6$ at which position the cellulose decomposition starts and consumes a lot of heat energy. Therefore, when the heat of pyrolysis is considered in the simulation, the temperature of biomass increases much slower as most energy is supplied to the cellulose decomposition. The result implies that the biomass fast pyrolysis process in the reactor is a heat-limited process.

Experimental studies of biomass fast pyrolysis in the auger reactor indicates that the biomass is able to complete the conversion process in the reactor. However, as shown in Figure 4 (b), the biomass is only half converted in the simulation. The prediction deviation might be a result of over-estimated heat of reaction value in the Ranzi's kinetics [12]. Research of [17] suggests that the heat requirement for woody biomass fast pyrolysis is in the range of 200-400 J/g above 600 K reaction temperature, whereas the heat required for cellulose fast pyrolysis is over 1100 J/g as given in the Ranzi's kinetics. Further careful scrutiny of the heat of reaction parameter is required.

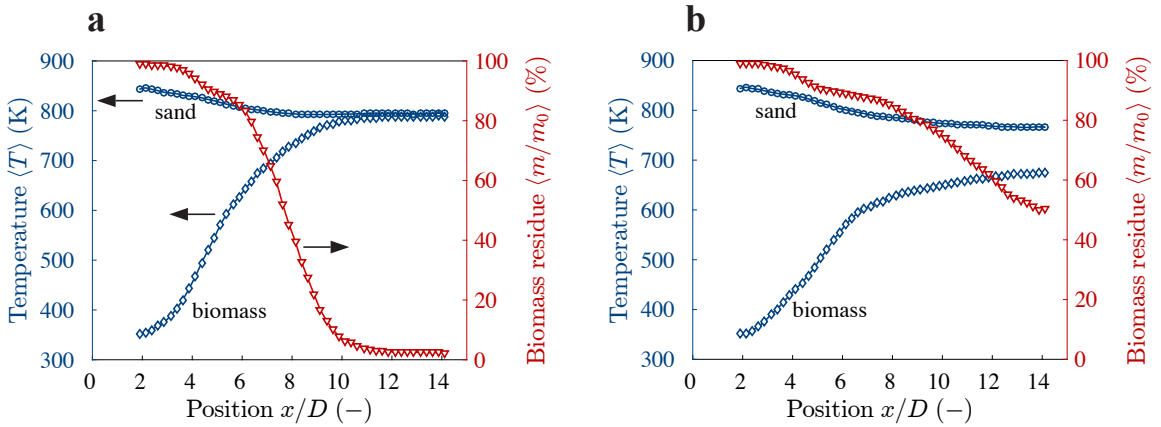

Figure 4: Predictions of biomass fast pyrolysis process in the reactor without heat of reaction (a) and with heat of reaction (b). Operating condition: particle size $d_p = 2$ mm, volumetric fill level $f = 0.1$, moisture content 10%.

3.2 Devolatilization dynamics of biomass components

Figure 5 shows the averaged mass loss rate of biomass major components: moisture, hemicellulose, cellulose and lignin. The hemicellulose mass is composed of origin hemicellulose and activated hemicellulose, the cellulose mass is the summation of origin cellulose and activated cellulose, and the lignin mass is composed of three original lignin forms (LIG-O, LIG-H, LIGC), carbon-rich lignin (LIGCC), OH-rich lignin (LIGOH) and lignin (LIG) as seen in Figure 2.

It is observed that the moisture evaporation reaches to the peak at the sand particle feed inlet at both high and low volumetric fill levels. But the duration of moisture evaporation at higher volumetric fill level ($f = 0.37$) increases. Both hemicellulose and lignin decomposition start around 480 K and cellulose starts to decompose around 600 K as clearly seen in Figure 5(a). This prediction is consistent with experimental observations in [16]. The prediction that cellulose reaches to its peak around 650 K also has a good agreement with previous research [16]. While the moisture evaporation is well separated from biomass decomposition in Figure 5 (a), the two processes have overlaps in Figure 5 (b). This behavior is believed to arise due to the non-ideal particle mixing and the resultant inhomogeneous particle heating temperature at higher volumetric fill level as have been discussed in our previous research [6, 7]. This is also why the initial decomposition temperature for cellulose seems to be lower in Figure 5 (b). The decomposition of all three components occurs in a relatively large temperature range due to the heat transfer limitations. The result also indicates a higher mass loss rate as decreasing volumetric fill level.

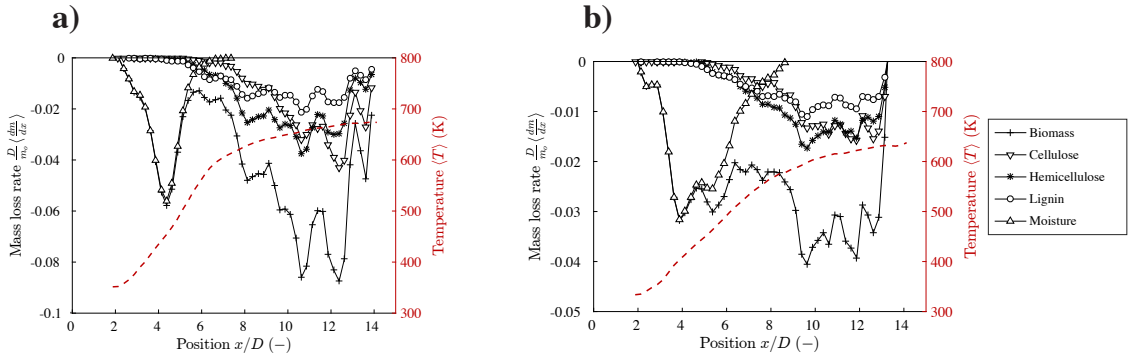

Figure 5: Non-dimensional mass loss rate of biomass major components. Operating condition: (a) particle size $d_p = 2$ mm, volumetric fill level $f = 0.1$; (b) $d_p = 2$ mm, $f = 0.37$. Moisture content is 10% in (a) and (b).

REFERENCES

[1] Stevens, C., Brown R.C. (2011). Thermochemical processing of biomass: conversion into fuels, chemicals and power. *John Wiley & Sons*.

[2] Goyal, H.B., Seal, D., Saxena R.C. (2008). Bio-fuels from thermochemical conversion of renewable resources: a review. *Renewable and sustainable energy reviews* 12(2), 504–517.

[3] Venderbosch, R.H., Prins, W. (2010). Fast pyrolysis technology development. *Biofuels, bioproducts and biorefining* 4(2), 178–208.

[4] Daugaard, T.J., Dalluge, D.L., Brown, R.C., Wright, M.M. (2018). Effect of thermophysical properties of heat carriers on performance of a laboratory-scale auger pyrolyzer. *Fuel processing technology* 176, 182–189.

[5] Liaw, S.S., Wang, Z., Ndegwa, P., Frear, C., Ha, S., Li, C.Z., Garcia-Perez, M. (2012) Effect of pyrolysis temperature on the yield and properties of bio-oils obtained from the auger pyrolysis of Douglas Fir wood. *Journal of Analytical and Applied Pyrolysis* 93, 52–62.

[6] Qi, F., Heindel, T.J., Wright, M.M. (2017). Numerical study of particle mixing in a lab-scale screw mixer using the discrete element method. *Powder technology* 308, 334–345.

[7] Qi, F., Heindel, T.J., Wright, M.M. (2018). Particle scale modeling of heat transfer in granular flows in a double screw reactor. *Powder technology* 335, 18–34.

[8] Aramideh, S., Xiong, Q., KOng, S.C., Brown, R.C.(2015) Numerical simulation of biomass fast pyrolysis in an auger reactor. *Fuel* 156, 234–242.

[9] Shi, X., Ronsse, F., Nachenius, R., Pieters, J.G. (2019) 3D Eulerian-Eulerian modelling of a screw reactor for biomass thermochemical conversion. Part 2: Slow pyrolysis for char production. *Renewable Energy* 143, 1477–1487.

[10] Brown, J.N., Brown, R.C. (2012). Process optimization of an auger pyrolyzer with heat carrier using response surface methodology. *Bioresource technology* 103(1), 405–414.

[11] Bryden, K.M., Hagge, M.J. (2003). Modeling the combined impact of moisture and char shrinkage on the pyrolysis of a biomass particle. *Fuel* 82(13), 1633–1644.

[12] Calonaci, M., Grana, R., Barker, H.E., Bozzano, G., Dente, M., Ranzi, E. (2010). Comprehensive kinetic modeling study of bio-oil formation from fast pyrolysis of biomass. *Energy & Fuels* 24(10), 5727–5734.

[13] Haseli, Y., Van Oijen, J.A., De Goey, L.P.H. (2011). Modeling biomass particle pyrolysis with temperature-dependent heat of reactions. *Journal of Analytical and Applied Pyrolysis* 90(2), 140–154.

[14] Kloss, C., Goniva, C., Hager, A., Amberger, S., Pirker, S. (2012). Models, algorithms and validation for opensource DEM and CFD–DEM. *Progress in Computational Fluid Dynamics, an International Journal* 12(2-3), 140–152.

[15] Ahnert, K., Mulansky, M. (2011). Odeint–solving ordinary differential equations in C++. *AIP Conference Proceedings* 1389(1), 1586–1589. AIP.

[16] Yang, H., Yan, R., Chen, H., Lee, D.H., Zheng, C. (2007). Characteristics of hemicellulose, cellulose and lignin pyrolysis. *Fuel* 86(12), 1781–1788.

[17] Van de Velden, M., Baeyens, J., Brems, A., Janssens, B., Dewil, R. (2010). Fundamentals, kinetics and endothermicity of the biomass pyrolysis reaction. *Renewable energy* 35(1), 232–242.